Identification of the Optimal Spectral Region for Plasmonic and Nanoplasmonic Sensing

Marinus A. Otte,[†] Borja Sepúlveda,[†,*] Weihai Ni,[‡] Jorge Pérez Juste,[‡] Luis M. Liz-Marzán,[‡] and Laura M. Lechuga[†]

[†]Nanobiosensors and Bioanalytical Applications Group, Research Centre in Nanoscience and Nanotechnology (CIN2) CSIC-ICN & CIBER-BBN, 08193 Bellaterra, Barcelona, Spain, and [‡]Departamento de Química Física and Unidad Asociada CSIC-Universidade de Vigo, 36310 Vigo, Spain

ABSTRACT We present a theoretical and experimental study involving the sensing characteristics of wavelength-interrogated plasmonic sensors based on surface plasmon polaritons (SPP) in planar gold films and on localized surface plasmon resonances (LSPR) of single gold nanorods. The tunability of both sensing platforms allowed us to analyze their bulk and surface sensing characteristics as a function of the plasmon resonance position. We demonstrate that a general figure of merit (FOM), which is equivalent in wavelength and energy scales, can be employed to mutually compare both sensing schemes. Most interestingly, this FOM has revealed a spectral region for which the surface sensitivity performance of both sensor types is optimized, which we attribute to the intrinsic dielectric properties of plasmonic materials. Additionally, in good agreement with theoretical predictions, we experimentally demonstrate that, although the SPP sensor offers a much better bulk sensitivity, the LSPR sensor shows an approximately 15% better performance for surface sensitivity measurements when its FOM is optimized. However, optimization of the substrate refractive index and the accessibility of the relevant molecules to the nanoparticles can lead to a total 3-fold improvement of the FOM in LSPR sensors.

KEYWORDS: surface plasmon resonance · localized surface plasmon resonance · sensing · biosensing · sensitivity · figure of merit · nanorods.

An important group of optical sensors is based on exploiting surface plasmon resonances (SPR) to detect small refractive index (RI) changes in close proximity to the sensing surface. Surface plasmons are generated at the interface between a metal and a dielectric. When this interface is planar, the plasmon can propagate in the form of an oscillating charge wave and is referred to as a surface plasmon polariton (SPP).[1] Excitation of an SPP with light of a suitable frequency, results in resonant energy transfer into the SPP, yielding a strong attenuation of the reflected signal when the sensor is optically interrogated. Spectroscopic analysis of this reflected signal therefore results in a dip-like response in the reflectivity spectrum. Sensors based on SPPs have been intensively studied and their use in medical diagnostics, environmental monitoring, food quality and safety analysis has been reported even using real samples.[2] Since they offer attractive properties such as real-time and label-free detection, SPP sensors have profiled themselves as the most widely employed and commercialized optical biosensors.[3]

Contrary to an SPP, a localized surface plasmon resonance (LSPR) is attributed to the resonant collective oscillation of the conduction electrons within a subwavelength metallic nanostructure.[4] The LSPR condition is strongly affected by the composition, size, shape and the surrounding dielectric environment of the nanostructure, the latter being the factor on which the sensing capabilities of nanoparticles rely.[5−7] Typically, the LSPR energies of metal nanostructures are located in the visible or near-infrared regions of the electromagnetic spectrum, and their resonantly enhanced extinction cross sections are sufficiently high to allow imaging and optical characterization of single particles by means of dark field scattering spectroscopy, resulting in peak-shaped spectral responses. Because of the possibilities that such measurements offer for miniaturization and multiplexing, LSPR-based sensing has attracted the interest of many researchers over the past decade.[4,8]

Although both sensing platforms offer specific advantages, their performance is mainly evaluated through their capability to detect changes in the monitored quantity (the refractive index), which ultimately determines the sensitivity (η) of the sensor. As both sensing schemes are generally characterized by a peak-shaped response, η can be defined as the shift of the peak position P_{SPR} upon dielectric changes in the environment, where P_{SPR} will be either the wavelength position λ_{SPR} or the energy position E_{SPR} of the resonance. When taking

*Address correspondence to borja.sepulveda@cin2.es.

Received for review August 17, 2009 and accepted November 23, 2009.

Published online November 30, 2009.
10.1021/nn901024e

biosensing considerations into account, it should be noted that, typically, the electromagnetic fields used as sensing probes in SPP and LSPR detection penetrate deeper into the dielectric than the usual layer thicknesses of adsorbed biomolecules. For the propagating plasmon, this effect is much more pronounced, with decay lengths varying between 100 and 500 nm,[9] whereas for a single nanorod, according to our simulations, (see Supporting Information), the sensitivity of the nanostructure saturates at a distance between 50 and 80 nm from the particle's surface, depending on the particle geometry. Therefore, distinction has to be made between bulk RI changes and local changes very close to the sensing surface.[10] In terms of sensitivity, this means that the bulk sensitivity (η_B) can be expressed as the variation of P_{SPR} per bulk RI (n_{bulk}) unit change:

$$\eta_B = \frac{\delta P_{SPR}}{\delta n_{bulk}} \quad (1)$$

On the other hand, the surface sensitivity (η_S) can be characterized as the P_{SPR} shift with respect to the thickness variation of an assembled thin layer (d_{bio}) (with a specific, constant RI) on top of the sensing substrate:

$$\eta_S = \frac{\delta P_{SPR}}{\delta d_{bio}} \quad (2)$$

A second factor affecting the sensing performance of the sensor is its resolving precision to detect changes of the monitored quantity. This parameter is typically represented by the full width at half-maximum (fwhm) of the resonance peak: a sharp peak facilitates the registration of a peak shift and *vice versa*.

Therefore, when considering the performance of a sensor, it is necessary to evaluate both sensitivity and peak width. A good example supporting this statement is the bulk sensitivity of LSPR-based sensors with the same geometry: analysis in wavelength scale reveals that whereas this quantity increases linearly when the resonance is red-shifted,[11] the peak width follows the same trend,[12] and therefore a trade-off is required to determine the optimized sensing region. A figure of merit (FOM), defined as

$$\mathrm{FOM} = \frac{\eta}{\mathrm{fwhm}} \quad (3)$$

correlates both quantities and can be used to quantify the general performance of a sensor and to allow comparison with that of other sensing schemes.[13] Also, a FOM neutralizes the controversy that may arise when comparing sensitivities and fwhm values in wavelength and energy scales, as we demonstrate here.

Theoretical and experimental studies on sensitivities of wavelength-interrogated SPP sensors have been reported,[2] and this investigation has recently been extended to the field of nanoparticle-based sensing platforms.[10,11,14,15] In this work, we present a comparative theoretical and experimental analysis, involving the sensing features of wavelength interrogated SPP sensors and LSPR sensors based on single nanoparticles with rodlike geometry, with the aim of extracting a general trend, valid for all plasmonic sensors. We take advantage of the spectral tunability of these systems to study their bulk and surface sensitivities as a function of plasmon resonance position. For both sensing schemes, we obtained FOMs for bulk and surface sensitivities, which revealed that the FOMs in wavelength and energy scales are equivalent and that an optimized spectral sensing range can be established for plasmonic sensors, which can be ascribed to the intrinsic plasmonic spectral properties of gold. First, we discuss bulk and surface sensitivity theoretical simulations, subsequently followed by an analysis involving the substrate effect on the sensitivity of immobilized nanorods. Next, we present the experimental results that confirm the theoretical findings. Again, the bulk sensitivity of both sensing schemes is discussed first, followed by the outcome of the surface sensitivity measurements.

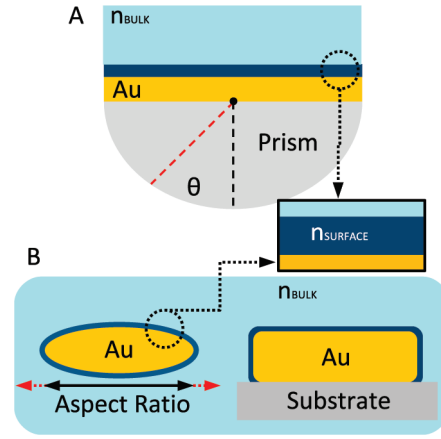

Figure 1. Schematic representation of both SPP (A) and LSPR (B) sensing schemes. The SPP Kretschmann setup consists of a gold sensing substrate, sandwiched between a prism and a bulk dielectric medium (n_{BULK}). Contrary, the LSPR sensing platform is modeled as a gold nanoellipsoid (MLWA) or a gold nanorod (FDTD) embedded in a dielectric environment (n_{BULK}). Surface sensitivity measurements are simulated by modeling a thin layer ($n = 1.50$) over the sensing substrates of both sensor types.

RESULTS AND DISCUSSION

Theoretical Predictions. The bulk and surface sensitivities for both SPP- and LSPR-based sensing methods were simulated according to the schematic models depicted in Figure 1. For the SPP sensors we considered a Kretschmann configuration with a glass prism ($n = 1.52$) and a sensing substrate composed of a 1.5 nm titanium sticking layer and a 50 nm gold layer, resembling the commercially obtained substrates used in the experiments. On the other hand, for the LSPR analysis

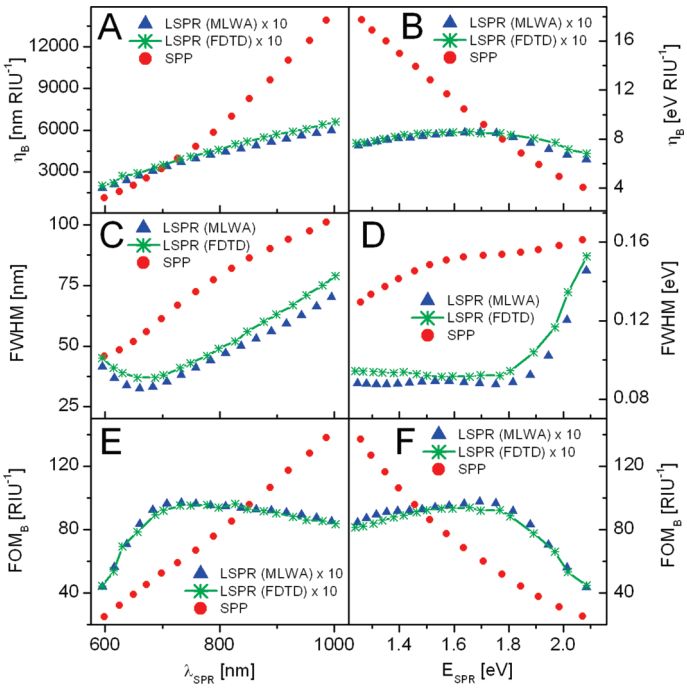

Figure 2. Calculated bulk sensitivity η_B, fwhm, and the corresponding FOM for both SPP (red circles) and LSPR sensing platforms in wavelength (A,C,E) and energy (B,D,F) scales. For the LSPR-based sensor, results obtained with both the MLWA (blue triangles) and the FDTD method (green crosses) are included. All data points are plotted *vs* resonance wavelength (λ_{SPR}) and energy (E_{SPR}).

we simulated rodlike gold nanoparticles of different aspect ratios. The selection of this morphology was motivated by the wide spectral tunability of gold nanorods while keeping small particle volumes, thus minimizing dephasing effects. In this theoretical analysis, gold nanoparticles were modeled following two different approaches: first, an ellipsoidal geometry was assumed through implementation of a modified long-wavelength approximation model (MLWA),[16] which enabled us to analytically calculate the polarizability of these nanostructures; second, we accurately reproduced the experimental nanorod morphology as spherically capped cylinders and implemented it in a rigorous finite-difference time-domain (FDTD) method, in which both the finite size of the particles and the effect of the substrate on the sensing performance of the particles are considered. The peak positions of both sensing systems were spectrally tuned between 600 and 1000 nm by changing either the incidence angle (64−78 degrees) of the incident light beam (SPP) or the aspect ratio (2−6) of the modeled nanorods (LSPR). In both sensing schemes, simulations of bulk sensitivity were carried out by varying the RI of the surrounding dielectric, whereas surface sensitivity was tested modeling the coating of a 1 nm thick uniform shell layer (n = 1.50) on the sensing substrate (see Figure 1). As previously mentioned, in FDTD the substrate (n = 1.52) was considered for both bulk and surface sensitivity simulations (see Methods section for details).

Figure 2 summarizes the results obtained from the bulk sensitivity simulations for both SPP and LSPR sensing schemes. The plots on the left-hand panel depict the normalized bulk sensitivity η_B, fwhm, and the corresponding FOM values in wavelength scale as a function of peak position λ_{SPR}, while the graphs on the right-hand panel represent the same quantities, but converted to energy scale.

When comparing the bulk sensing performance of both sensor types, analysis of η_B in terms of wavelength (Figure 2A) shows, for both configurations, a roughly linear increase as the peak position is redshifted. This effect is due to the longer penetration of the electromagnetic (EM) field inside the dielectric at longer resonant wavelengths, thus providing a larger volume that is sensitive toward RI changes (see Supporting Information). Additionally, comparison of η_B between both sensing schemes reveals that the sensitivity calculated for SPP sensors is roughly 1 order of magnitude larger than that of their LSPR counterparts. Again, this difference can be explained by a much longer penetration depth of the confined EM field in the external dielectric medium for SPP-based sensors. For the LSPR, comparison of MLWA and FDTD methods shows that both the trends and the obtained values for η_B, fwhm, and FOM are approximately the same. Therefore, as long as the characteristic size of the nanoparticle is kept small compared to the wavelength of light and the nanoparticle is embedded in an homogeneous dielectric medium, the MLWA approach is justified and can be safely used to examine the sensing performance of these nanostructures, exploiting this method's much shorter calculation times compared to FDTD simulations.

However, if we mutually compare sensitivity and fwhm values between wavelength and energy scales (Figure 2A−D), controversy may arise. For example, in the wavelength domain, the LSPR bulk sensitivity monotonically increases with λ_{SPR}, whereas in the energy plot the slope changes at $E_{SPR} \approx 1.75$ eV. When considering the fwhm, the observed trends are even more controversial. In this case, SPP sensors show larger peak widths for higher values of E_{SPR}, whereas wavelength representation suggests that lower resonance wavelengths are accompanied by narrower peaks. Also, for the LSPR sensing scheme, an abrupt fwhm increase is observed at a threshold value of $E_{SPR} \approx 1.8$ eV, whereas for smaller energies the peak width is more or less constant; this shows very little resemblance with the fwhm change in the wavelength scale.

All this apparent controversy can be eliminated by using the FOM as the parameter of choice, since it can

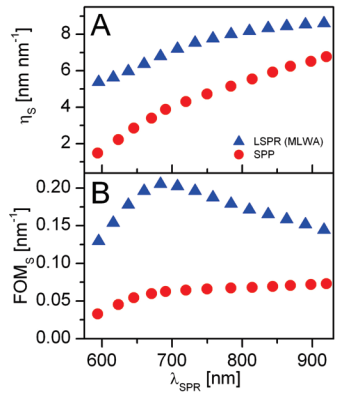

Figure 3. Calculated surface sensitivities η_S (A) and the corresponding FOMs (B) for the SPP (red circles) and the LSPR (blue triangles for MLWA and green stars for FDTD) sensing platforms as a function of spectral position of resonant wavelength λ_{SPR}.

be mathematically demonstrated that the FOM in energy and wavelength domains are approximately equivalent (see Supporting Information). Such equivalency is confirmed in the calculated results shown in Figure 2E,F. From these values we can see that the bulk FOM of SPP sensors is roughly 1 order of magnitude larger than that of LSPR sensors, even though the overall peak widths in the latter are substantially smaller. For SPP sensors, the bulk FOM exhibits a linear behavior, from which it can be deduced that the performance of this sensor improves at longer resonance wavelengths, that is, lower excitation energies. In contrast, examination of the LSPR bulk FOM reveals a different trend, with the FOM showing a maximum located at $\lambda_{SPR} \approx 700$ nm, corresponding to $E_{SPR} \approx 1.75$ eV. Close to this value, the balance between sensitivity and resolution is maximized, resulting in an optimized sensing region. Note that from this point on, with FOM-equivalency established in energy and wavelength regimes, all figures displaying sensitivity, fwhm, or FOM values will only be plotted in wavelength scale.

From a biosensing point of view, surface sensitivity and surface FOM are the relevant parameters to describe the sensing performance and, as shown in Figure 3, this can result in a very different behavior when compared to the bulk sensitivity calculations. Examination of η_S shows that the spectral shifts of the LSPR for the analyzed wavelength range are larger than those calculated for the SPP configuration. For both sensor types, surface sensitivity consistently increases as λ_{SPR} is red-shifted, though also in both cases the slope gets smaller at longer λ_{SPR}. Again, because the evanescent field has an increased penetration depth into the dielectric at longer λ_{SPR}, the EM-field is expected to be less confined near the surface and thus the sensitivity will decrease.

Due to the higher η_S values and lower peak widths obtained for the LSPR sensors, their FOM values are typically higher than those for their SPP counterparts. As in the bulk sensitivity simulations, the surface FOM

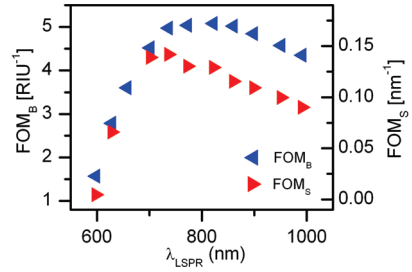

Figure 4. Bulk and surface sensitivities of the LSPR sensing scheme for nanorods modeled on top of a glass substrate, calculated with the FDTD method.

of the LSPR sensor displays a maximum, again located at $\lambda_{SPR} \approx 700$ nm. However, for the SPP sensor, the FOM values increase as λ_{SPR} is red-shifted, though signs of saturation become apparent for SPR wavelengths above $\lambda_{SPR} \approx 700$ nm, and a slight decrease for $\lambda_{SPR} >$ 1000 nm was noted (not shown). When comparing the FOM maxima of both sensing schemes, a 3-fold increase in surface FOM was found for the LSPR sensor, reflecting the stronger confinement of the EM field around the plasmonic nanostructures.

From these bulk and surface calculations, we can conclude that, although superior bulk sensing performance was found for the SPP device, a better surface sensing performance is expected for the LSPR-based sensing platform. Furthermore, the observed maximum surface FOM values suggest the existence of an optimum spectral sensing range for both LSPR and SPP sensors. For SPP sensors a broad optimum region can be defined between 700 and 1000 nm, whereas a narrower optimum spectral range around an excitation wavelength of 700 nm is predicted for LSPR sensing.

However, we have so far considered that the metal nanoparticles are surrounded by a uniform dielectric medium and are homogenously coated with a thin dielectric layer. However, for practical biosensing applications, attachment of the nanoparticles to a solid substrate is required, thus allowing in-flow assays, kinetic analysis, surface regeneration, and multiplexing. The substrate, which generally has a higher RI than the sensing environment (the solvent), can significantly hinder the sensing performance of the nanoparticles. To identify and quantify the effect of the substrate on the performance of the LSPR-based sensing scheme, we carried out FDTD calculations of the bulk and surface sensitivities of single gold nanorods lying on top of a silica substrate ($n = 1.52$). For the surface sensitivity simulations, only the part of the nanorod contacting the substrate was excluded from the modeling of a 1 nm thick layer with a RI of 1.50, resulting in a total surface coverage larger than 95%. The resulting bulk and surface FOMs are displayed in Figure 4. Although the observed trends for the FOM remain unchanged, the bulk sensitivity shows that, indeed, the actual calculated values are significantly lower as compared to those obtained for particles entirely surrounded by a

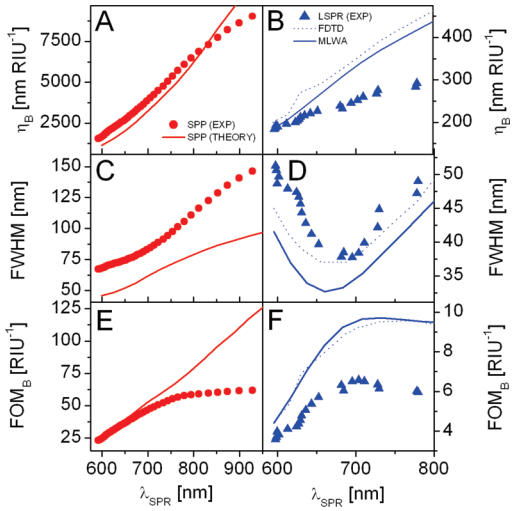

Figure 5. Experimental results of the bulk sensitivity measurements carried out on the SPP (red dots: A,C,E) and LSPR (blue triangles: B,D,F) sensors. The solid and dashed lines represent the corresponding theoretical values, according to Figure 2. The bulk sensitivity η_B, fwhm, and FOM were plotted as a function of the spectral position of the resonance peak λ_{SPR}.

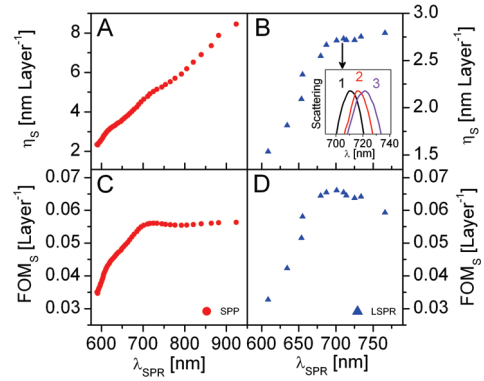

Figure 6. Experimental results representing the surface sensitivity η_S and the accompanying FOM as a function of λ_{SPR} for both SPP (A, C) and LSPR (B, D) sensing schemes. The inset in panel B shows the spectral peak shifts as a consequence of the deposition of PDDA/PSS bilayers for a gold nanorod.

homogeneous dielectric medium, resulting in a 40% decrease of the bulk sensitivity. However, the surface sensitivity is approximately equal due to the almost complete surface coverage assumed in the calculations.

In an effort to confirm these theoretical findings and elucidate the effects of the substrate on the final sensitivity of the LSPR systems, we carried out a systematic experimental study on both SPP and LSPR sensors.

Experiments. To compare the experimental bulk and surface sensitivities of SPP and LSPR sensors we employed an SPP sensing setup in Kretschmann configuration,[17] which allowed us to spectrally tune the SPP resonance by varying the light incidence angle. Within an angle range between 64 and 78 degrees, we were able to tune the SPP resonance between 600 and 900 nm. For the LSPR sensing platform, tunability was achieved by using gold nanorods with aspect ratios ranging from 2 up to 4.5, allowing us to spectrally tune the resonance between 600 and 800 nm. These nanoparticles, fabricated by wet chemistry (see Methods), were immobilized on glass substrates *via* electrostatic interactions, using polyelectrolytes, and the scattering spectra from single nanoparticles were acquired using dark-field microspectroscopy.[18]

Bulk sensitivity measurements were carried out by gradually varying the RI of the external dielectric medium (see Supporting Information). Figure 5 shows the results of these experiments for SPP (A,C,E) and LSPR (B,D,F). For both sensing platforms, η_B was found to linearly increase as λ_{SPR} was red-shifted. Furthermore, the obtained bulk sensitivity of the SPP sensor is an order of magnitude larger than that of its LSPR counterpart. Regarding peak widths, similar trends in the fwhm of the SPP and LSPR sensors compared to the theoretical calculations were obtained, except for the long wavelength region of the SPP sensor. Such differences stem from the Kretschmann excitation of the surface plasmon in the SPP sensor with a hemicylindrical prism (see Supporting Information) and explain the apparent saturation of the FOM in this region (see Figure 5E). However, an overall quantitative agreement between theory and experiment in the FOM was obtained. On the other hand, a substantial experimental reduction of η_B and FOM can be appreciated for the results on nanoparticles when compared to the theoretical calculations of these nanostructures surrounded by a uniform dielectric medium (Figure 2), but accurately matching the predicted results of the FDTD calculations for nanorods on a substrate (Figure 4). The 40% reduction of the bulk sensitivity with respect to the nanoparticles in a homogeneous medium confirms that the nanorods "see" a smaller effective RI change as compared to the induced external RI change, as a consequence of the high refractive index of the substrate and the concentration of a substantial part of the near field of the nanorods within the glass region.

Interestingly, as indicated from the theoretical analysis, the gathered experimental results evidence that, for bulk RI measurements, the FOM of gold nanorod-based sensors exhibits a maximum at approximately $\lambda_{SPR} = 700$ nm. However, from the much longer spectral shifts obtained for the SPP sensor, one can establish that these sensors clearly outperform the LSPR sensors in bulk RI detection.

The surface sensitivity of both sensing platforms was investigated through the in-flow deposition of poly(diallyldimethylammonium chloride) (PDDA) and poly(sodium 4-styrenesulfonate) (PSS) polyelectrolyte monolayers (layers RI $\approx$ 1.50),[19] exploiting the ability of such polyelectrolytes to create conformal multilayers on planar or nanostructured solid substrates. The results of these measurements are illustrated in Figure 6, where η_s and the corresponding surface FOM,

averaged over four monolayers, are displayed for both sensor configurations. As an example of these measurements, the inset of Figure 6B shows the induced peak shifts as a consequence of the successive deposition of two polymer bilayers for a nanorod with longitudinal surface plasmon peaking at 711 nm in water.

As becomes clear from the figure, SPP and LSPR sensors show a monotonic growth of η_s over the analyzed wavelength range, and their FOMs exhibit the expected optimized sensing region for resonances located around 700 nm, confirming what was already perceived in the theoretical simulations: this maximum in the FOM defines an optimized surface sensing region for plasmonic sensing, where the ratio between the induced spectral shifts and the losses due to internal damping mechanisms is optimized. This allows for the *a priori* optimal determination of the rod geometry or the incidence angle, in order to fully exploit the surface sensing performance of these systems, as also has been considered by Nusz *et al*. for nanoparticles.[20]

The spectral peak shifts of the SPP sensor range from approximately 2 to 8 nm per assembled polyelectrolyte monolayer. Assuming that the refractive index of the polyelectrolytes is 1.50, a thickness around 1 nm per monolayer of polyelectrolyte can be estimated from the measurements, which permits a direct comparison with the theoretical values of the surface sensitivities and FOMs.

These measurements show a drastically lower surface sensitivity for the nanoparticles, since their spectral shifts vary between 1.5 and 3 nm per polymer monolayer. This means a 60% drop of surface sensitivity and FOMs with respect to the theoretical calculations. However, we should remember that in the calculations, a surface coverage of the nanorods larger than 95% was assumed, whereas the experimentally achieved surface coverage can be substantially smaller, around 50% or even lower. Such considerable surface coverage reduction can be due to the electrostatic repulsion generated by the molecules attached to the surface, which hinder access to the region between nanorod and glass substrate.

This effect is very likely to be present in biosensing applications, especially for larger biomolecules, such as proteins, unless the substrate is totally inert to unspecific adsorption. Despite of the large reduction of the surface sensitivity in the LSPR sensing scheme, the overall narrower peaks compared to SPP sensor are ultimately responsible for the resulting higher surface FOM values for the LSPR sensors. Hence, we can conclude that, for surface sensitivity measurements, nanorod-based sensors have offered approximately 15% better performance than their SPP counterpart when their FOM was maximized. However, even larger FOM values could be achieved by improving the access of target molecules to the active sensing surface of the nanoparticles, toward the 3-fold enhancement predicted in the theoretical calculations. This can be envisaged through positioning gold nanoparticles on dielectric nanopillars,[21] or using low refractive index and inert substrates, such as fluoropolymers.[22] Another noteworthy alternative to increase the sensor performance involves the use of silver as the plasmonic material, since its lower absorption compared to gold guarantees higher FOM values.

Judging from the surface FOM of both sensor types we can conclude that a substantial improvement of the sensor performance can be achieved by simply separating the resonance wavelength from the gold interband transitions. However, as a consequence of the optimized sensing region, no additional benefit is obtained by red-shifting the resonance indefinitely toward the infrared, which in addition involves complicating the detection systems, especially for single particle sensing. In this respect, colloidal nanorods probably offer the best sensing features in terms of sensitivity and resolution due to their particularly narrow peaks. For the same reasons, nanospheres are poor candidates for LSPR sensing, since the red-shift required to achieve higher sensitivity is accompanied by strong dephasing damping. When compared to the widely employed SPP biosensor, these results support the viable use of this LSPR-based sensing scheme in biosensing applications. However, for nanoplasmonic sensors, biosensing detection should be kept within 10−15 nm from the surface. Beyond that distance, the sensitivity is strongly damped, thus limiting the biosensing application to small molecules and advising against, for example, sandwich assays.

In an attempt to determine the origin of these optimized spectral sensing ranges, we analyze here the optical properties of plasmonic materials. In an ideal metal, the spectral plasmonic behavior is restricted to a spectral range between two boundaries: the high energy limit, given by the plasma frequency, and the low energy limit in which the metal starts acting as a perfect conductor. Above the plasma frequency, the dielectric constant of the metal becomes positive, thus preventing the excitation of surface plasmons. On the other hand, for low energies, the penetration of the EM fields in the metal is very weak and the plasmonic behavior is lost. Accordingly, between these boundaries, one can expect a spectral range in which plasmons exhibit an optimized performance.

From the analysis of the resonance conditions of both sensor types, it can be concluded that the real part of the dielectric constant ε_{Re} of the metal determines the spectral position of the resonance and according to Miller and Lazarides[11] the bulk sensitivity also depends linearly on ε_{Re}, while the imaginary part ε_{Im} is responsible for the damping. Since the FOM is a measure for the trade-off between the spectral shifts (spectral position of the resonance) and the peak widths (damping), we propose that the maximum of the

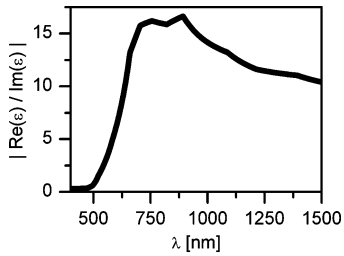

Figure 7. Absolute values of the ratio between real and imaginary parts of the dielectric constant of gold, displayed as a function of the wavelength λ of light.

$\varepsilon_{Re}/\varepsilon_{Im}$ ratio should coincide with the optimal sensing areas as extracted from the FOMs. Figure 7 depicts the absolute value of this ratio as a function of wavelength using the optical properties of gold employed for our calculations. From this figure we can extract a peak-shaped trend with a range of maximum values located between approximately 700 and 900 nm, indicating that it is in this region, where the ratio between the sensitivity and the fwhm is optimized.

A more detailed derivation supporting this statement can be obtained starting off from a Drude model for free electrons, which represents the archetypical model of plasmonic materials. From the ratio between the real and imaginary parts of the dielectric constant, an analytical equation of the maximum value of $\varepsilon_{Re}/\varepsilon_{Im}$ can be derived, given by (see Supporting Information):

$$\lambda_{max} = \frac{\sqrt{3\varepsilon_\infty}\Gamma\lambda_p}{\sqrt{\Gamma^2 - \varepsilon_\infty\lambda_p^2}} \quad (4)$$

In eq 4 ε_∞ (dimensionless) is the dielectric constant of the metal at infinite frequency, Γ (nm) is a measure for the damping of the oscillation, and λ_p (nm) is the plasma wavelength of the metal. If we assume $\varepsilon_\infty = 8.786$, $\Gamma = 16496$ nm, and $\lambda_p = 139.9$ nm, which fit gold optical constants for wavelengths longer than 550 nm (see Supporting Information), a maximum located at 718.5 nm is found. When comparing this wavelength to the sensing FOMs, we can see that it closely corresponds to the position of the maximum derived from the LSPR FOMs and the start of the saturation observed in the SPP surface FOM. Therefore, we conclude that the overall behavior of these FOMs can be attributed to the intrinsic optical properties of the plasmonic material.

CONCLUSIONS

We presented comparative theoretical and experimental analyses of the sensing performance of wavelength-interrogated plasmonic sensors based on propagating and localized surface plasmon resonances. We exploited the tunability of both sensing platforms to spectrally vary the resonances in order to analyze their bulk and surface sensing characteristics as a function of their resonance position. A FOM, which relates the sensitivity and resolving power of the sensing platforms, was used to extract a general behavior for these plasmonic sensor types. We demonstrated FOM equivalency in both wavelength and energy scales. Furthermore, the FOM corresponding to the surface sensitivity of both sensing schemes revealed the existence of an optimized spectral sensing range, which we assign to the intrinsic optical properties of the employed plasmonic material. For the LSPR sensor, this optimized sensing region corresponds to nanorods with excitation resonances close to $\lambda_{SPR} = 700$ nm. On the other hand, the SPP sensor exhibits a broader optimized surface sensing region comprising resonance wavelengths between 700 and 1000 nm. Although the SPP sensor clearly benefits from higher bulk sensitivity when compared to its LSPR counterpart, the latter sensor type has proven a 15% better surface sensitivity performance. However, theoretical calculations suggest that a 3-fold improvement of the FOM could be achieved for metal nanoparticles by improving the access of the molecules to the sensing surface.

METHODS

Optical Constants. Optical constants of gold reported by Johnson and Christy[23] were used for the calculations. Modeling of the titanium sticking layer in the SPP simulations was carried out using optical constants retrieved from Weber.[24]

SPP Simulations. To model SPP based sensors, a transfer matrix formalism was employed to calculate the reflectivity of a TM polarized EM wave impinging at the sensing substrate at a single incidence angle,[25] using a Kretschmann configuration:[17] prism as incident medium ($n = 1.52$), 1.5 nm titanium sticking layer with a 50 nm gold layer on top (resembling commercially obtained substrates used in the experiments), and water as the sensing medium ($n = 1.33$). The surface sensitivity was modeled by coating the metal layer with a 1 nm thick dielectric layer ($n = 1.5$). The bulk sensitivity was normalized by dividing the difference in peak position with the difference in refractive index. The surface sensitivity was evaluated by comparing the peak positions with and without the modeled coating layer on top of the substrate. FWHMs were measured at the half intensity of the peak maximum.

MLWA Calculations. Interaction of metal nanoparticles with light was investigated through implementation of the modified long-wavelength approximation (MLWA).[16] This method permits the use of the electrostatic approximation for nanoparticles with typical sizes up to 10% of the wavelength of light. This is achieved by introducing corrections for radiative damping and depolarization of the collective electron oscillation. Although in the experiments rod-shaped particles were measured, in the simulations we opted for an ellipsoidal geometry, since for this geometry an analytical expression for the polarization can be derived.[26] Using the aspect ratio of the particle as a variable, while maintaining the two short-axes of the particle at 20 nm, we were able to spectrally tune the LSPR. Bulk and surface sensitivity simulations were carried out as previously discussed for the SPP simulations.

FDTD Calculations. Nanorods were modeled as cylinders caped by hemispheres. A mesh size of 2 nm was used in the bulk sensitivity calculations in a homogeneous medium, whereas 0.5 nm mesh was used to model the surface sensitivity of the nanorods and the calculations with the glass substrate. The width of the

nanorods was fixed at 20 nm. Only the longitudinal plasmon resonance of Au nanorods was calculated by setting the electric field of the plane wave parallel to the longitudinal direction of the Au nanorods. To investigate substrate effects, an edge of the nanorod was contacted to a modeled substrate ($n = 1.52$). For surface sensitivity simulations of the rods in the presence of a substrate, the overlapping part of the dielectric coating with the substrate was overridden by the substrate. After calculation, the positions of the resonance peaks in the scattering spectra were located. Bulk and surface sensitivity parameters were obtained in the same manner as done in the SPP simulations.

SPP Experiments. Commercially available gold substrates (50 ± 2 nm Au, 1.5 ± 0.3 nm Ti) were cleaned immersing them briefly in a freshly prepared 3:1 piranha solution (H_2SO_4/H_2O_2), prior to attachment onto a hemicylindrical glass prism *via* refractive index matching oil for the Kretschmann configuration. This part of the setup was attached to a motorized rotary plate, allowing the system to rotate with respect to a fixed halogen light source (HL-2000, Mikropack), such that the incidence angle of the collimated incoming TM-polarized light could be varied. A corrective lens system, rotating along the same axis, was used to collect the reflected light leaving the prism with a multimode optical fiber. Finally, a spectrometer (Shamrock SR-303i, Andor) connected to a cooled CCD detector (Newton, Andor) was used to analyze the collected light. For the bulk sensitivity measurements, mixtures of H_2O and a saline buffer were prepared covering a range of values of the RI varying between $n = 1.3325-1.3415$. Injection of these samples into the flow cell allowed us to analyze the SPR spectra as a function of both the bulk RI and the incidence angle of the incoming light. For the surface sensitivity measurements, PDDA and PSS polymer ($M_w < 100000$) solutions (2 wt %) were prepared. Making use of electrostatic affinity of PDDA to both gold and PSS, subsequent injection of PDDA and PSS resulted in the in-flow formation of polyelectrolyte multilayers on top of the gold substrate.

LSPR Experiments. Gold nanorods were prepared following the Ag^+-assisted method proposed by Nikoobakht *et al.*[27] and modified by Liu *et al.*[28] Briefly, first a gold seed solution was prepared by borohydride reduction of 5 mL of 0.25 mM $HAuCl_4$ in an aqueous 0.1 M CTAB solution. For the synthesis of the gold nanorods, 24 μL of seed solution was added to a growth solution containing 0.1 M CTAB, 0.5 mM $HAuCl_4$, 0.75 mM ascorbic acid, and 0.12 mM silver nitrate and in the presence or the absence of 0.019 M HCl. The nanorods thus synthesized have an average length, width, and aspect ratio of 72.1 ± 10.2, 19.0 ± 2.9, and 3.86 ± 0.77 nm and 53.0 ± 8.1, 21.3 ± 3.1, and 2.52 ± 0.46 nm, respectively. The nanorods were electrostatically attached to glass slides. Briefly, after piranha ($3H_2SO_4/1H_2O_2$) cleaning, the glass slides were incubated for 2 min in a PDDA 2 wt % solution, followed by extensive water rinsing, yielding the formation of a PDDA monolayer on top of the glass slide. Gold nanorods with varying aspect ratios and coated with PSS were then deposited following the same incubation procedure as described above. Subsequently, the samples were placed in an ozone generator for 10 min, to remove all the remaining organic compounds. Finally, a new PDDA monolayer was deposited for stability purposes. An inverted microscope (Eclipse Ti−U, Nikon) equipped with a halogen 100 W light source and fiber-coupled to the above-mentioned spectrometer, was utilized to obtain the elastic scattering spectra of single nanoparticles by means of dark field microscopy. Two different dark field condensers (Dry NA 0.90−0.80 and Oil NA 1.43−1.20, Nikon), in combination with a 100× oil immersion objective (Plan Fluor 100× NA 0.5−1.3 Oil, Nikon) were employed to collect light scattered by single nanoparticles. A Teflon flow cell, sealed by two glass slides, one of them containing the immobilized nanorods, was employed to carry out the sensitivity measurements. For surface sensitivity studies, polyelectrolyte multilayers were deposited in-flow, through the alternating injection of 2 wt % PDDA and PSS solutions. Elastic scattering spectra of single nanorods were obtained at a slow continuous flow of water after each polyelectrolyte bilayer deposition.

Acknowledgment. This research was carried out with the support of the Commission for Universities and Investigation belonging to the Department of Innovation, Universities and Companies of the Generalitat de Catalunya, and the Social European Fund. Financial support of the M. Botín Foundation and the Nanomag CIBER-BBN Project is also greatly acknowledged. L.M.L.-M. acknowledges financial support from Ministerio de Ciencia e Innovación (MAT2007-62696 and PCI2005-A7-0075).

Note added in proof: During the review of this manuscript, a highly relevant article has been published: Svedendahl, M.; Chen, S.; Dmitriev, A.; Käll, M. Refractometric Sensing Using Propagating *versus* Localized Surface Plasmons: A Direct Comparison. *Nano Lett.*, published online October 20, 2009, http://dx.doi.org/10.1021/nl902721z.

Supporting Information Available: Detailed derivations of the reported analytical formulas and details of the SPP setup explaining the observed increasing slope of the peak widths at higher resonance wavelengths are supplied. This material is available free of charge *via* the Internet at http://pubs.acs.org.

REFERENCES AND NOTES

1. Maier, S. A. *Plasmonics: Fundamentals and Applications*; Springer: New York, 2007.
2. Homola, J. Surface Plasmon Resonance Sensors for Detection of Chemical and Biological Species. *Chem. Rev.* **2008**, *108*, 462–493.
3. Lechuga, L. M. *Biosensors and Modern Biospecific Analytical Techniques*; Elsevier Science: New York, 2005; Vol. 44.
4. Sepúlveda, B.; Angelomé, P. C.; Lechuga, L. M.; Liz-Marzán, L. M. LSPR-Based Nanobiosensors. *Nano Today* **2009**, *4*, 244–251.
5. Liz-Marzán, L. M. Tailoring Surface Plasmons through the Morphology and Assembly of Metal Nanoparticles. *Langmuir* **2006**, *22*, 32–41.
6. Jensen, T. R.; Malinsky, M. D.; Haynes, C. L.; Van Duyne, R. P. Nanosphere Lithography: Tunable Localized Surface Plasmon Resonance Spectra of Silver Nanoparticles. *J. Phys. Chem. B* **2000**, *104*, 10549–10556.
7. Jensen, T. R.; Duval, M. L.; Kelly, K. L.; Lazarides, A. A.; Schatz, G. C.; Van Duyne, R. P. Nanosphere Lithography: Effect of the External Dielectric Medium on the Surface Plasmon Resonance Spectrum of a Periodic Array of Silver Nanoparticles. *J. Phys. Chem. B* **1999**, *103*, 9846–9853.
8. Anker, J. N.; Hall, W. P.; Lyandres, O.; Shah, N. C.; Zhao, J.; Van Duyne, R. P. Biosensing with Plasmonic Nanosensors. *Nat. Mater.* **2008**, *7*, 442–453.
9. Homola, J. Present and Future of Surface Plasmon Resonance Biosensors. *Anal. Bioanal. Chem.* **2003**, *377*, 528–539.
10. Murray, W. A.; Auguieì, B.; Barnes, W. L. Sensitivity of Localized Surface Plasmon Resonances to Bulk and Local Changes in the Optical Environment. *J. Phys. Chem. C* **2009**, *113*, 5120–5125.
11. Miller, M. M.; Lazarides, A. A. Sensitivity of Metal Nanoparticle Surface Plasmon Resonance to the Dielectric Environment. *J. Phys. Chem. B* **2005**, *109*, 21556–21565.
12. Novo, C.; Gomez, D.; Pérez-Juste, J.; Zhang, Z.; Petrova, H.; Reismann, M.; Mulvaney, P.; Hartland, G. V. Contributions from Radiation Damping and Surface Scattering to the Linewidth of the Longitudinal Plasmon Band of Gold Nanorods: A Single Particle Study. *Phys. Chem. Chem. Phys.* **2006**, *8*, 3540–3546.
13. Sherry, L. J.; Chang, S.-H.; Schatz, G. C.; Van Duyne, R. P.; Wiley, B. J.; Xia, Y. Localized Surface Plasmon Resonance Spectroscopy of Single Silver Nanocubes. *Nano Lett.* **2005**, *5*, 2034–2038.
14. Kvasnièka, P.; Homola, J. Optical Sensors Based on Spectroscopy of Localized Surface Plasmons on Metallic Nanoparticles: Sensitivity Considerations. *Biointerphases* **2008**, *3*, FD4−FD11.
15. Malinsky, M. D.; Kelly, K. L.; Schatz, G. C.; Van Duyne, R. P. Nanosphere Lithography: Effect of Substrate on the Localized Surface Plasmon Resonance Spectrum of Silver Nanoparticles. *J. Phys. Chem. B* **2001**, *105*, 2343–2350.

16. Jensen, T.; Kelly, L.; Lazarides, A.; Schatz, G. C. Electrodynamics of Noble Metal Nanoparticles and Nanoparticle Clusters. *J. Cluster Sci.* **1999**, *10*, 295–317.
17. Kretschmann, E. Die Bestimmung Optischer Konstanten von Metallen durch Anregung von Oberflächenplasmaschwingungen. *Z. Phys.* **1971**, *241*, 313–324.
18. Sönnichsen, C.; Franzl, T.; Wilk, T.; von Plessen, G.; Feldmann, J.; Wilson, O.; Mulvaney, P. Drastic Reduction of Plasmon Damping in Gold Nanorods. *Phys. Rev. Lett.* **2002**, *88*, 077402−1−077402−4.
19. Richert, L.; Arntz, Y.; Schaaf, P.; Voegel, J.-C.; Picart, C. pH Dependent Growth of Poly(L-lysine)/Poly(L-glutamic) Acid Multilayer Films and Their Cell Adhesion Properties. *Surf. Sci.* **2004**, *570*, 13–29.
20. Nusz, G. J.; Curry, A. C.; Marinakos, S. M.; Wax, A.; Chilkoti, A. Rational Selection of Gold Nanorod Geometry for Label-Free Plasmonic Biosensors. *ACS Nano* **2009**, *3*, 795–806.
21. Dmitriev, A.; Hägglund, C.; Chen, S.; Fredriksson, H.; Pakizeh, T.; Käll, M.; Sutherland, D. S. Enhanced Nanoplasmonic Optical Sensors with Reduced Substrate Effect. *Nano Lett.* **2008**, *8*, 3893–3898.
22. Brian, B.; Sepúlveda, B.; Alaverdyan, Y.; Lechuga, L. M.; Käll, M. Sensitivity Enhancement of Nanoplasmonic Sensors in Low Refractive Index Substrates. *Opt. Exp.* **2009**, *17*, 2015–2023.
23. Johnson, P. B.; Christy, R. W. Optical Constants of the Noble Metals. *Phys. Rev. B.* **1972**, *6*, 4370–4379.
24. Weber, M. J. *Handbook of Optical Materials*; CRC: New York, 2002.
25. Schubert, M. Polarization-Dependent Optical Parameters of Arbitrarily Anisotropic Homogeneous Layered Systems. *Phys. Rev. B.* **1996**, *53*, 4265–4274.
26. Bohren, C. F.; Huffman, D. R. *Absorption and Scattering of Light by Small Particles;* Wiley-Interscience: Weinheim, Germany, 1998.
27. Nikoobakht, B.; El-Sayed, M. A. Preparation and Growth Mechanism of Gold Nanorods (NRs) Using Seed-Mediated Growth Method. *Chem. Mater.* **2003**, *15*, 1957–1962.
28. Liu, M.; Guyot-Sionnest, P. Mechanism of Silver(I)-Assisted Growth of Gold Nanorods and Bipyramids. *J. Phys. Chem. B* **2005**, *109*, 22192–22200.